ELSEVIER

Surface Science 364 (1996) 131–140

surface science

Electron differential inverse mean free path for surface electron spectroscopy

Y.F. Chen [a,*], C.M. Kwei [b]

[a] *Precision Instrument Development Center, National Science Council, 20 R&D Road VI, Science-based Industrial Park, Hsinchu, Taiwan*
[b] *Department of Electronics Engineering, National Chiao Tung University, Hsinchu, Taiwan*

Received 13 October 1995; accepted for publication 19 February 1996

Abstract

A new, general expression for the position-dependent differential inverse mean free path (DIMFP) of an electron penetrating into vacuum from a solid is derived. This DIMFP can be divided up into a bulk and a surface term. It is found that the surface effect is restricted to a surface layer extending on both sides of the vacuum–solid interface. An extended Drude dielectric function, which allows the characteristic oscillator strength, damping constant, and critical-point energy for each subband of valence electrons, is employed to estimate electron DIMFPs near Al and Au surfaces. Our results are relevant to the understanding of inelastic electron scattering near a solid surface.

Keywords: Electron–solid interactions, scattering; Photoelectron spectroscopy

1. Introduction

X-ray photoelectron spectroscopy (XPS) and Auger electron spectroscopy (AES) are widely used to study surface composition from analysis of the emitted electron spectrum [1–6]. The surface sensitivity of these techniques arises from the fact that electron inelastic mean free paths in solids are short, on the order of a few atomic spacings [7–10], for electron energies between 100 eV and 2 keV.

The energy distribution of electrons emitted from a solid surface is distorted due to inelastic scattering and background subtraction is necessary before any quantitative spectral analysis can be performed [11–16]. To subtract the inelastic background signal from measured energy spectra, detailed knowledge of the differential inverse mean free path (DIMFP) for inelastic scattering is essential [17–22]. In addition, the DIMFP is also important for the evaluation of electron slowing down. Nevertheless, the theoretical DIMFP adopted to analyze surface electron spectra is quite primitive. The DIMFP derived from an electron traveling in an infinite solid is usually used to describe the inelastic interactions of surface electron spectroscopies. This DIMFP, which does not take account of effects intrinsic to the solid surface, is spatially non-varying within the solid.

In view of recent studies on angle-resolved XPS and reflection electron-energy loss spectroscopy (REELS) [23–28], surface effects are very important for electrons of energies ranging from a few hundred to 2000 eV and especially for glancing

* Corresponding author. Fax: +886-35 773947; e-mail: yfchen@pidc.gov.tw.

PII S0039-6028(96)00616-4

escape electrons. Previously, Feibelman [29,30] estimated the electron inverse mean free path (IMFP) near a metal surface by employing the step-function electron-gas density profile within the high-frequency limit of the random-phase approximation (RPA), in which plasmon dispersion is neglected. He pointed out that the IMFP is dependent on the actual depth underneath the solid surface and scattering is not confined to the interior of the solid. Besides, Kitagawa [31] derived the spatial dependence of the stopping power for an inhomogeneous many-electron system by use of the Dirac density matrix formalism. However, to the knowledge of these authors, the position dependence of the DIMFP near a solid surface has never been investigated. In our recent study, we have successfully included surface effects in the quantitative analysis of XPS by the differential surface excitation parameter (DSEP) [32] which is defined as the probability of a single loss event resulting from surface effects for an electron crossing a solid surface. Even so, the possibility that an electron may be liberated at a depth in the solid within the effective region of surface effects has not been described by the DSEP.

In this work, we have used dielectric theory to derive the DIMFP formula for electrons emerging from a solid surface. It was found that the DIMFP for electrons near a solid surface can be split up into a bulk and a surface term. The bulk term is simply the well-known expression of the DIMFP in an infinite medium, while the surface term is restricted to a surface layer extending on both sides of the vacuum–solid interface. The inelastic interactions of the escape electron with the solid can even take place while the electron is outside the solid. This surface effect will influence the energy distribution of the escape electron, especially in the spectra of electrons originating near the surface. For the purposes of illustration, we have employed an extended Drude dielectric function [10] to calculate electron DIMFPs near Al and Au surfaces.

2. Theory

The inelastic interactions between emitted electrons and solid electrons in a medium comprise mainly bulk and surface excitations. Electrons near the surface are responsible primarily for surface excitations, while those deep inside contribute mostly to bulk excitations. These inelastic interactions can be described in terms of the dielectric function of the solid.

Even though the specular-reflection model introduced by Ritchie and Marusak [33] is known to reproduce many properties of real surfaces very well, the knowledge of the electrodynamics of non-specular surfaces is needed in the case of XPS and AES. In this work, we shall study the cases of an electron crossing the surface of a semi-infinite medium at oblique incidence with a velocity v. The surface will be chosen at the plane $z=0$ with the z axis in the perpendicular direction from the solid with dielectric function $\epsilon(q,\omega)$ to the vacuum. The notation $v=|\boldsymbol{v}|$, $\boldsymbol{q}=(\boldsymbol{Q},q_z)$, $\boldsymbol{v}=(\boldsymbol{v}_\parallel,v_z)$, and $\boldsymbol{r}=(\boldsymbol{R},z)$, *where* $\boldsymbol{Q}$, $\boldsymbol{v}_\parallel$, and $\boldsymbol{R}$ represent the corresponding components parallel with the interface, will be adopted hereafter. Note that atomic units are used through this work, unless otherwise specified.

For an electron with velocity v crossing the surface at $t=0$ from the solid $\epsilon(\boldsymbol{q},\omega)$ to the vacuum the Fourier components of the scalar electric potential may be given by

$$\phi^{(s)}(\boldsymbol{q},\omega)=\frac{-8\pi^2}{q^2\epsilon(\boldsymbol{q},\omega)}[\delta(\omega-\boldsymbol{q}\cdot\boldsymbol{v})+\rho_s(\boldsymbol{Q},\omega)] \quad z<0 \tag{1}$$

$$\phi^{(v)}(\boldsymbol{q},\omega)=\frac{-8\pi^2}{q^2}[\delta(\omega-\boldsymbol{q}\cdot\boldsymbol{v})+\rho_s(\boldsymbol{Q},\omega)] \quad z>0. \tag{2}$$

The first terms in Eqs. (1) and (2) represent the charge density of the moving electron and $\rho_s(\boldsymbol{Q},\omega)$ is the amplitude of the fictitious surface charge which is required to satisfy the requisite boundary conditions. The opposite sign of the second term between Eq. (1) and Eq. (2) originates from the requirement of continuity of the electric displacement. Matching $\phi^{(s)}(z=-0)$ and $\phi^{(v)}(z=+0)$ yields the required $\rho_s(\boldsymbol{Q},\omega)$ as

$$\rho_s(\boldsymbol{Q},\omega)=\frac{Q}{\pi}\frac{|v_z|}{\tilde{\omega}^2+(v_zQ)^2}\frac{\bar{\epsilon}(\boldsymbol{Q},\omega)}{\epsilon(\tilde{\boldsymbol{q}},\omega)}\frac{\epsilon(\tilde{\boldsymbol{q}},\omega)-1}{\bar{\epsilon}(\boldsymbol{Q},\omega)+1} \tag{3}$$

where

$$\frac{1}{\bar{\epsilon}(\boldsymbol{Q},\omega)} = \frac{Q}{\pi}\int_{-\infty}^{\infty}\frac{\mathrm{d}q_z}{q^2\epsilon(\boldsymbol{q},\omega)}, \tag{4}$$

$\tilde{\omega} = \omega - v_{\parallel}\cdot\boldsymbol{Q}$ and $\tilde{q}^2 = Q^s + \tilde{\omega}^2/v_z^2$. In terms of $\rho_s(\boldsymbol{Q},\omega)$, the induced scalar potential is obtained from Eqs. (1) and (2) as

$$\phi_{\mathrm{ind}}(\boldsymbol{r},t) = \frac{-1}{2\pi^2}\int \mathrm{d}\omega \int \mathrm{d}^3\boldsymbol{q}\,\frac{\mathrm{e}^{i(\boldsymbol{q}\cdot\boldsymbol{r}-\omega t)}}{q^2} \times\left\{\rho_s(\boldsymbol{Q},\omega)\left[\frac{\Theta(-z)}{\epsilon(\boldsymbol{q},\omega)} - \Theta(z)\right] + \delta(\omega-\boldsymbol{q}\cdot\boldsymbol{v})\Theta(-z)\left[\frac{1}{\epsilon(\boldsymbol{q},\omega)}-1\right]\right\}, \tag{5}$$

where $\Theta(z)$ is the Heaviside step function.

The stopping power is given by [34]:

$$-\frac{\mathrm{d}W}{\mathrm{d}s} = \frac{1}{v}\left[\frac{\partial\phi_{\mathrm{ind}}(\boldsymbol{r},t)}{\partial t}\right]_{\boldsymbol{r}=\boldsymbol{v}t}, \tag{6}$$

where the derivative of ϕ_{ind} is evaluated at the position of the electron, $\boldsymbol{r} = \boldsymbol{v}t$. From Eqs. (5) and (6) we get the stopping power of the solid for the electron

$$-\frac{\mathrm{d}W}{\mathrm{d}s} = \frac{i}{2\pi^2 v}\int \omega\,\mathrm{d}\omega \int \mathrm{d}^2\boldsymbol{Q}\left\{\frac{\pi}{Q}\rho_s(\boldsymbol{Q},\omega)\,\mathrm{e}^{-i\tilde{\omega}z/v_z} \times\left[\frac{\Theta(-z)}{\bar{\epsilon}(z,\boldsymbol{Q},\omega)} - \mathrm{e}^{-Q|z|}\Theta(z)\right] + \frac{|v_z|}{\tilde{\omega}^2+(v_zQ)^2}\Theta(-z)\left[\frac{1}{\epsilon(\tilde{\boldsymbol{q}},\omega)}-1\right]\right\}, \tag{7}$$

where

$$\frac{1}{\bar{\epsilon}(z,\boldsymbol{Q},\omega)} = \frac{Q}{\pi}\int_{-\infty}^{\infty}\frac{\mathrm{d}q_z\,\mathrm{e}^{iq_zz}}{q^2\epsilon(q,\omega)}. \tag{8}$$

The evaluation of the first term in the curly bracket of Eq. (7) depends on sgn z, as this determines whether the ω-integration must be performed by closing through the upper (U) or lower (L) half-plane (HP). For $z<0$, i.e., the electron inside the solid $\epsilon(\boldsymbol{q},\omega)$ and approaching the surface, we must close the integration contour through the UHP. On the other hand, for $z>0$, i.e., the electron inside the vacuum and moving away from the surface, the integration contour must be closed through the LHP. This integration contour involves the poles of $\rho_s(\boldsymbol{Q},\omega)$ and $1/\bar{\epsilon}(\boldsymbol{Q},\omega,z)$ which approach the real axis from below and give the surface and bulk excitation modes of the solid, respectively. For simplicity it is convenient to use the identity [35]

$$\mathrm{e}^{-i\tilde{\omega}z/v_z} = 2\cos(\tilde{\omega}z/v_z) - \mathrm{e}^{i\tilde{\omega}z/v_z}. \tag{9}$$

The integration containing the complex exponential on the right-hand side of Eq. (9) can then be performed again through the UHP. Therefore, Eq. (7) can be written as

$$-\frac{\mathrm{d}W}{\mathrm{d}s} = \frac{1}{\pi^2 v}\int_0^{\infty}\mathrm{d}\omega\int \mathrm{d}^2\boldsymbol{Q}\,\frac{\omega|v_z|}{\tilde{\omega}^2+(v_zQ)^2} \times \mathrm{Im}\left[\Pi(\boldsymbol{v},z,\boldsymbol{Q},\omega) - \frac{\Theta(-z)}{\epsilon(\tilde{\boldsymbol{q}},\omega)}\right], \tag{10}$$

where

$$\Pi(\boldsymbol{v},z,\boldsymbol{Q},\omega) = \mathrm{e}^{-Q|z|}\left[\frac{\Theta(-z)}{\bar{\epsilon}(z,\boldsymbol{Q},\omega)} - (2\cos(\tilde{\omega}z/v_z) - \mathrm{e}^{-Q|z|})\Theta(z)\right] \times\left[-\frac{\bar{\epsilon}(\boldsymbol{Q},\omega)}{\epsilon(\tilde{\boldsymbol{q}},\omega)}\,\frac{\epsilon(\tilde{\boldsymbol{q}},\omega)-1}{\bar{\epsilon}(\boldsymbol{Q},\omega)+1}\right], \tag{11}$$

corresponds to the spatially varying surface energy loss function. In the derivation we have used the property $\epsilon(-\boldsymbol{q},-\omega) = \epsilon^*(\boldsymbol{q},\omega)$.

For an electron of energy $E = v^2/2$ to loss energy ω, the spatially varying differential inverse mean free path (DIMFP), $\mu(E\to E-\omega,\alpha,z)$, can be related to the stopping power as follows:

$$-\frac{\mathrm{d}W}{\mathrm{d}s} = \int_0^{\infty}\omega\mu(E\to E-\omega,\alpha,z)\,\mathrm{d}\omega, \tag{12}$$

where α is the angle between the electron velocity and positive z-axis. This definition of α will be used hereafter.

From Eqs. (10)–(12), the DIMFP for electrons near a vacuum–solid surface can be split up into a bulk and a surface term:

$$\mu(E\to E-\omega,\alpha,z) = \mu_B(E\to E-\omega) + \mu_S(E\to E-\omega,\alpha,z) \tag{13}$$

where

$$\mu_B(E\to E-\omega)=\frac{1}{\pi^2 v}\int d^2\boldsymbol{Q}\frac{|v_z|}{\tilde{\omega}^2+(v_zQ)^2}\times \mathrm{Im}\left[-\frac{\Theta(-z)}{\epsilon(\tilde{\boldsymbol{q}},\omega)}\right], \quad (14)$$

and

$$\mu_S(E\to E-\omega,\alpha,z)=\frac{1}{\pi^2 v}\int d^2\boldsymbol{Q}\frac{|v_z|}{\tilde{\omega}^2+(v_zQ)^2}\times \mathrm{Im}[\Pi_s(\boldsymbol{v},z,\boldsymbol{Q},\omega)]. \quad (15)$$

The bulk term, which is independent of the position and emission angle, gives rise to the well-known expression of the DIMFP of electrons moving in an infinite medium [36]. On the other hand, the surface term is dependent on z and α. It was found that the interaction of the electron with the solid is not confined to the interior of the solid, but also takes place while the electron is at some distance outside the surface.

Neglecting the effect of spatial dispersion of the medium, a local dielectric function $\epsilon(\omega)$ could be used to describe the response of the medium. From Eq. (4) and Eq. (8) we easily obtain

$$\bar{\epsilon}(\boldsymbol{Q},\omega)=\epsilon(\tilde{q},\omega)=\epsilon(\omega), \quad (16)$$

and

$$\bar{\epsilon}(z,\boldsymbol{Q},\omega)=\epsilon(\omega)\,e^{Q|z|}. \quad (17)$$

Substituting Eqs. (16) and (17) into Eq. (13), after some algebra, we find

$$\begin{aligned}\mu(E\to E-\omega,\alpha,z)&=\frac{1}{\pi^2 v}\int d^2\boldsymbol{Q}\frac{|v_z|}{\tilde{\omega}^2+(v_zQ)^2}\left\{\mathrm{Im}\left(\frac{-2}{\epsilon(\omega)+1}\right)e^{-Q|z|}\times\left[2\cos\left(\frac{\omega z}{v_z}\right)-e^{-Q|z|}\right]\Theta(z)\right.\\&\left.+\left[\mathrm{Im}\left(\frac{-2}{\epsilon(\omega)+1}\right)e^{-2Q|z|}+\mathrm{Im}\left(\frac{-1}{\epsilon(\omega)}\right)(1-e^{-2Q|z|})\right]\Theta(-z)\right\}. \quad (18)\end{aligned}$$

Note that the surface effect for $z<0$, i.e., inside the solid, as first pointed out by Ritchie [36] is twofold: a surface mode appears, via the term $\mathrm{Im}(-2/\epsilon(\omega)+1)\,e^{-2Q|z|}$, while, on the other hand, a reduction in loss due to bulk excitation of modes is introduced via the term $\mathrm{Im}(-1/\epsilon(\omega))(1-e^{-2Q|z|})$. At the surface, the DIMFP for bulk plasmon excitation vanishes, due to the orthogonality of bulk and surface plasmons. Eq. (18) also reveals that only the surface mode exists outside the solid.

Since there is the $e^{-Q|z|}$ term in Eq. (11) for $\Pi_s(v,z,\boldsymbol{Q},\omega)$, surface effects have a rather limited extent about the surface. The effective region extends into the solid to a depth of about v/ω_p, where ω_p is the plasmon energy [37]. Since ω_p lies in the interval 20–35 eV, the depth is roughly around 3–6 Å for a 1 keV electron. Accordingly, we may expect that most emitted electrons penetrate this effective region. Thus, surface effects can approximately be characterized by the differential surface excitation parameter (DSEP) which can be calculated via integration of Eq. (15), i.e.,

$$P_S(E\to E-\omega,\alpha)=\int_{-\infty}^{\infty}\frac{dz}{\cos\alpha}\mu_S(E\to E-\omega,\alpha,z). \quad (19)$$

The surface excitation parameter (SEP) for an electron crossing a vacuum–solid surface is then given by [37]:

$$P_S(E,\alpha)=\int_0^E P_S(E\to E-\omega,\alpha)\,d\omega. \quad (20)$$

Using a local dielectric function and carrying out the integration over $\boldsymbol{Q}$ and z, the DSEP can be simplified:

$$P_S(E\to E-\omega,\alpha)=\frac{1}{2v\cos\alpha}\frac{1}{\omega}\mathrm{Im}\left[\frac{(1-\epsilon(\omega))^2}{\epsilon(\omega)(1+e(\omega))}\right]. \quad (21)$$

Substituting the free-electron-gas dielectric function,

$$\epsilon(\omega)=1-\frac{\omega_p^2}{\omega(\omega+i\gamma)}\quad \gamma\to 0^+, \quad (22)$$

into Eqs. (20) and (21), we get

$$P_S(E,\alpha) = \frac{\pi}{4v}\frac{1}{\cos\alpha}, \tag{23}$$

which shows that the surface excitation probability is proportional to $(\cos\alpha)^{-1}$ [38]. This angular dependence has been verified experimentally for large α values [39]. Eq. (23) seems to imply that the DIMFP $\mu_S(E\to E-\omega,\alpha,z)$ in the integrand of Eq. (19) is approximately α independent. This property has been confirmed by the result of numerical calculations. Taking $\alpha = 0°$ in Eq. (23), we obtain the results of Ritchie [36] for normal incident electrons.

So far, the derived formulae have not taken into account the recoil effect which arises from the recoil term appearing in the conservations of energy and momentum. Based on the conservation of energy and momentum this effect can be included by limiting the range of integration over $\boldsymbol{Q}$ as follows:

$$q_-^2 \le \left(\frac{\tilde{\omega}}{v_z}\right)^2 + Q^2 \le q_+^2, \tag{24}$$

where $q_\pm = \sqrt{2E} \pm \sqrt{2(E-\omega)}$.

The model dielectric used in this work is identical to that used previously. Here we present a brief synopsis for the purpose of completeness. The real and imaginary parts of the dielectric function are given by [5,39–41]:

$$\epsilon_1(q,\omega) = \epsilon_b - \sum_i \frac{A_i[\omega^2 - (\omega_i + q^2/2)^2]}{[\omega^2 - (\omega_i + q^2/2)^2] + (\omega\gamma_i)^2} \tag{25}$$

and

$$\epsilon_2(q,\omega) = \sum_i \frac{A_i\gamma_i\omega}{[\omega^2 - (\omega_i + q^2/2)^2]^2 + (\omega\gamma_i)^2}, \tag{26}$$

where A_i, γ_i, and ω_i are, respectively, the oscillator strength, damping coefficient, and critical-point energy, all associated with the ith interband transition. Note that we include a ϵ_b term to account for the background dielectric constant due to the influence of polarizable atomic cores [42]. The values of these parameters were determined by a fit of Eq. (26), in the limit $q\to 0$, to the experimental optical data. To make sure that the fitted parameters are accurate, we require that the model dielectric function satisfies two sum rules, i.e.,

$$\int_0^{\hat{\omega}} \omega\epsilon_2(0,\omega)\,d\omega = \frac{\pi}{2}\sum_i A_i = \frac{\pi}{2}\omega_p^2 \tag{27}$$

and

$$\int_0^{\hat{\omega}} \omega\,\mathrm{Im}\left[\frac{-1}{\epsilon(0,\omega)}\right] d\omega = \frac{\pi\omega_p^2}{2\epsilon_b^2}, \tag{28}$$

where ω_p is the bulk plasmon energy of valence electrons and $\hat{\omega}$ is an energy cutoff, large compared to the valence-band excitations but well below the energy of the inner-shell transitions responsible for the dispersive dielectric background.

It is worthwhile mentioning that we have used a common approximation in deriving the present result wherein the surface response of the semi-infinite solid is expressed in terms of the bulk dielectric function $\epsilon(\boldsymbol{q},\omega)$ via Eq. (1). This approximation is exact for $Q=0$ and has been labeled quasiclassical or step density. It arose originally in surface-plasmon theory [33], but has had a widespread use in surface response problems since then. For $Q\neq 0$, Feibelman [43,44] has shown that the charge-density profile at the surface affects the properties of the surface response function, such as the surface-plasmon dispersion. Nevertheless, the exact dependence of the dielectric function on momentum transfer is seldom known, an extrapolation from the optical limit to other momentum transfers must be made. The expression adopted in Eqs. (25) and (26) for the q-dependence works correctly at the two ends of the momentum transfer, i.e., the optical end, $q\to 0$, and the Bethe ridge region, $q\to\infty$ [41]. Eq. (24) indicates that the range of integration over $\boldsymbol{Q}$ is rather large for electron energies larger than a few hundred electronvolts, therefore the actual dispersion relationship makes only minor differences in the determination of DIMFP [10,32].

3. Results and discussion

On the basis of the model dielectric function, we have calculated the DIMFPs for electrons emitted from solid surfaces. The parameters in the model

dielectric function have been obtained in our previous work [10]. Although the DIMFP is dependent on the position and emission angle, the angular dependence is indeed rather weak. Therefore, all results presented here are for the case of electrons emerging along the surface normal. Figs. 1 and 2 show the energy loss dependence of the calculated DIMFPs for an escaping electron with an energy of 500 eV at various positions inside Au and Al, respectively. It can be seen that the structures and peak positions of DIMFPs vary with the actual depth underneath the solid surface. Slightly inside the solid, the DIMFP quickly approaches the result of electrons moving in an infinite solid, which indicates that the surface effect is restricted to a limited region. However, details in the Au band structure give rise to a multitude of possible electronic excitations, and consequently, the DIMFP is a broad function of the energy loss. Although surface plasmon excitations contribute largely at small energy losses as compared to bulk plasmon excitations, the broadness results in the strong overlapping between bulk and surface plasmon excitations. Therefore, for Au it is difficult to identify the relative contributions between bulk and surface plasmon excitations from the energy loss structures of the DIMFPs. In contrast, Al is a free electron-like metal and its DIMFP essentially shows a two-peak structure, as shown in Fig. 2. The peak energies at ~ 10 eV and ~ 15 eV

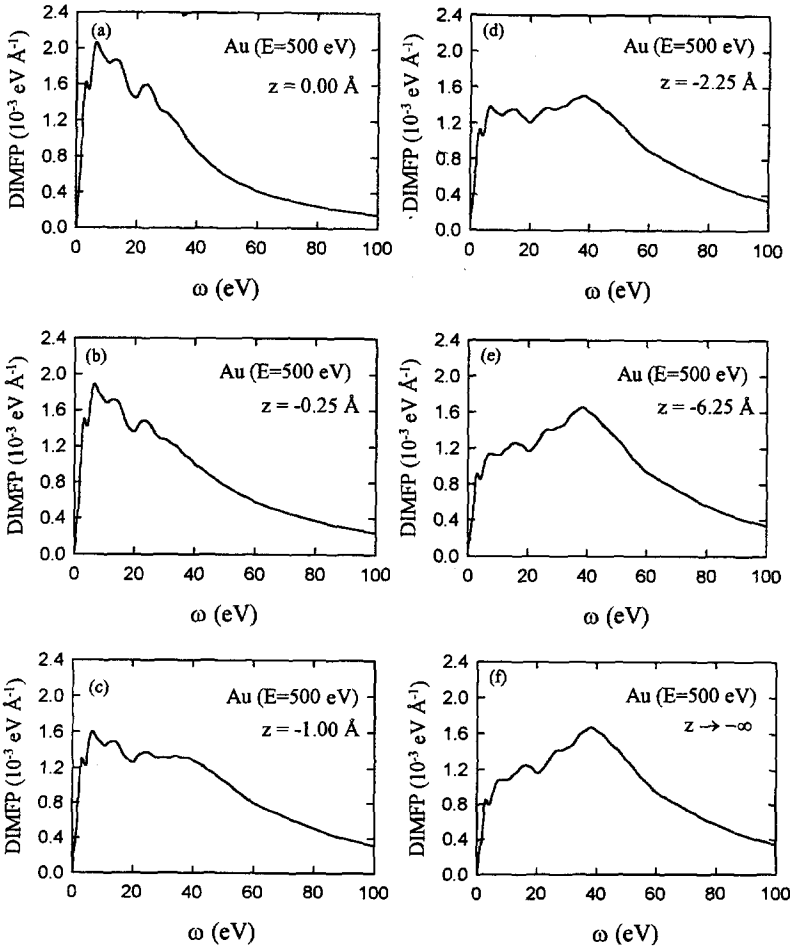

Fig. 1. A plot of the energy loss dependence of the calculated DIMFPs for a normally escape electron with 500 eV at various positions inside Au.

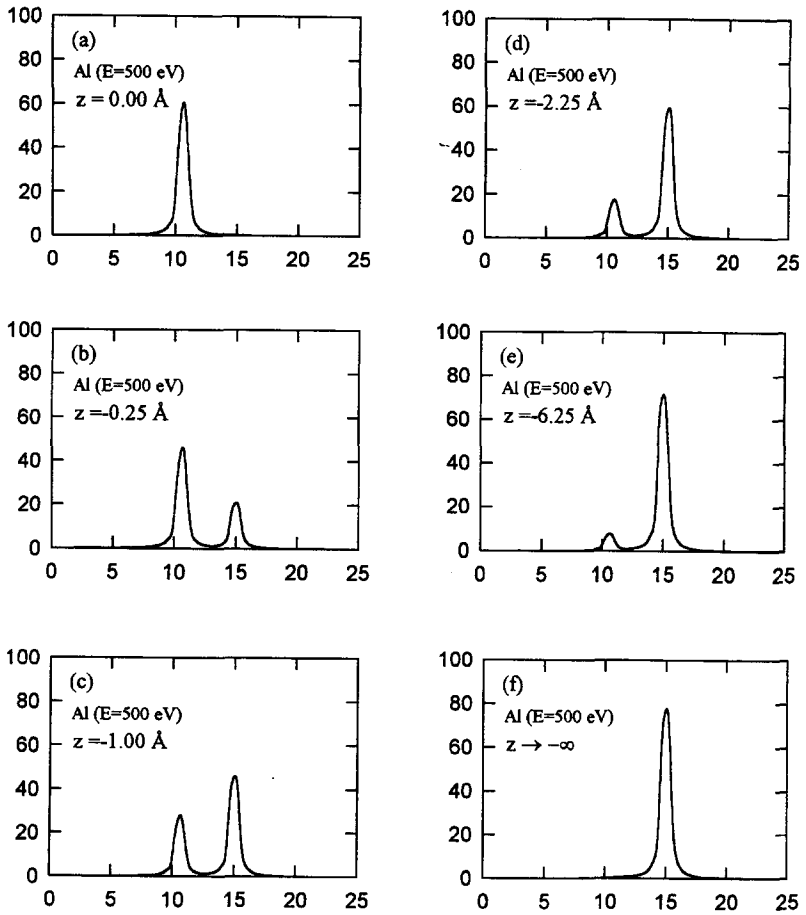

Fig. 2. A plot of the energy loss dependence of the calculated DIMFPs for a normally escape electron with 500 eV at various positions inside Al.

correspond to surface and bulk plasmon excitations, respectively. The result in Fig. 2 clearly shows that the probability of exciting a surface plasmon decreases and the probability of exciting a bulk plasmon increases with depth. Note at the surface, the DIMFP is pure for surface plasmon excitations due to the orthogonality of bulk and surface plasmons.

Fig. 3 shows the energy loss dependence of the DIMFPs for a normally escape electron with 500 eV at various positions outside Au. It is seen that the DIMFP curves get narrower and their values get smaller at a greater distance. Besides, the relative intensity of the peaks changes with the distance outside the surface. Since all escape electrons must travel the effective region at the vacuum side, surface effects will influence the energy distribution of the escape electron and should unavoidably lead to strong spectral structures, especially in the spectra of electrons originating near the surface, for which bulk effects are weak.

Fig. 4 shows the position dependence of the IMFPs for a 500 eV electron normally exiting from Al. To explore the surface effects, we also plot in this figure the IMFPs for bulk and surface plasmon excitations inside Al individually. We can see that an electron inside the solid can excite a surface plasmon near the surface, however, the orthogonality of bulk and surface plasmons compensates this increase via a reduction of the probability of bulk plasmon excitations. Therefore, the assumption of a spatially non-varying IMFP inside the surface is

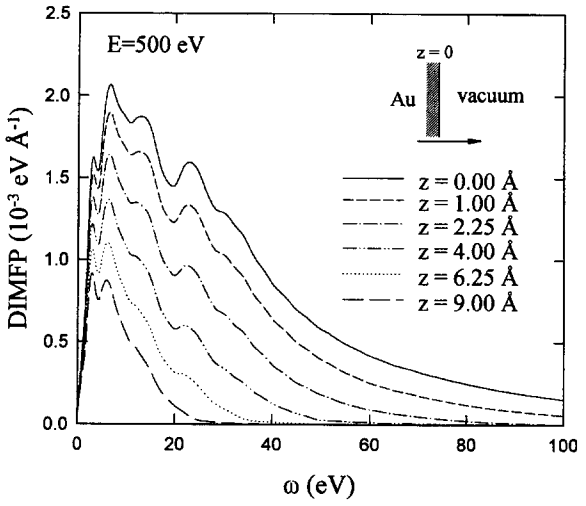

Fig. 3. A plot of the energy loss dependence of the DIMFPs for a normally escape electron with 500 eV at various positions outside Au.

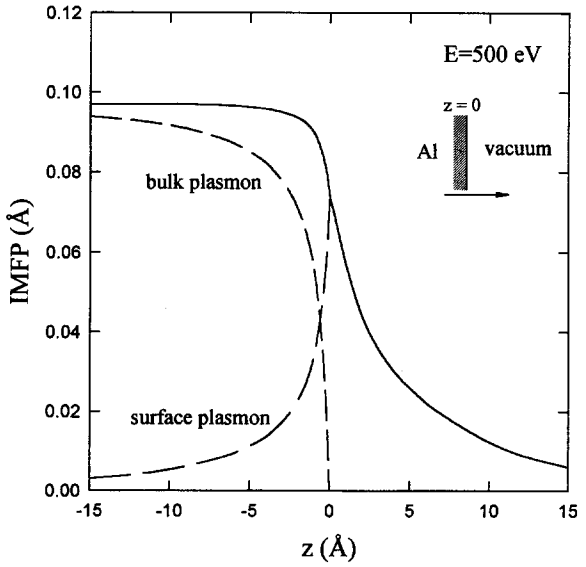

Fig. 4. A plot of the position dependence of the IMFPs for a 500 eV electron normally exiting from Al.

a reasonable approximation, as shown in Fig. 4. Nevertheless, one should keep in mind the fact that the DIMFP is dependent on the actual depth underneath the surface. Fig. 4 also shows that the IMFP for surface plasmon excitations is at a maximum at $z = 0$, and it decays to zero on either side of the surface at a distance on the order of Ångström. It can be seen that the effective region of the surface excitation at the vacuum side is slightly wider than that at the medium side. This asymmetric phenomenon arise from the different position dependences of the DIMFP on both sides. In view of Eq. (18), the position factors of surface plasmon excitations are $e^{-Q|z|}[2\cos(\omega z/v_z) - e^{-Q|z|}]$ and $e^{-2Q|z|}$ for outside and inside the solid, respectively. Finally, we show the position dependence of the IMFPs for electrons with several energies normally exiting from Au (Fig. 5). For all electron energies, the IMFP does not fall off to zero abruptly outside the surface, as shown in Fig. 4.

Inputting the present DIMFP into the Monte Carlo code, we have computed the Au 4f XPS spectra with a source function of mixed Lorentzian and Gaussian form fitted by Yoshikawa et al. [27]. Details of the Monte Carlo procedure are described elsewhere [45–47]. The generation of Au 4f photoelectrons along the paths of incident Al–Kα X-rays is traced to a depth of 100 Å. The computer program terminates when all electrons either leave the solid to the region where the surface effects are negligible or their energies fall below a cutoff energy of 1300 eV. Escaping electrons from the solid are then registered if they enter the acceptance

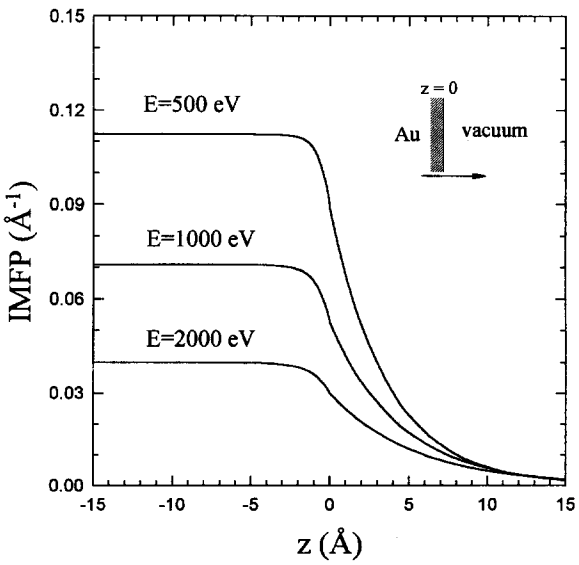

Fig. 5. A plot of the position dependence of the IMFPs for electrons with several energies normally exiting from Au.

solid angle of the analyzer. This solid angle corresponds to an acceptance angle within $\pm 4°$ from the central axis of the analyzer. Fig. 6 shows the Au 4f spectra calculated with (solid curve) and without (dashed curve) surface effects and the spectrum measured experimentally [28] (dotted curve) for different emission angles with respect to the surface normal (i.e., $\alpha = 0°$, 45°, and 75°). The angle between the X-ray source and the analyzer axis is 71°. Note that all data are magnified five times relative to the no-loss Au $4f_{7/2}$ peak. It shows that present results, including surface effects, agree very well with experimental data at all take-off angles, whereas the results without surface effects fail to describe the background intensity and energy-loss structure in the region below 30 eV. This sort of failure is also found in the results obtained by the Monte Carlo simulation method of Yoshikawa et al. [28] who neglected surface excitations. It is also seen that the influence of surface excitations is relatively more important at larger escape angles due to the increased surface excitation probability at these angles. The contribution from surface excitations to the XPS Au 4f spectra is significant for energy loss in the region below 30 eV. This is consistent with the results of the DIMFPs in Fig. 3. Although the present results are in agreement with the experimental data, some deviations still exist in all cases studied. These deviations may be due to neglecting the shake-off process which can be induced by the single-electron excitation [48] or by the intrinsic plasmon loss [49].

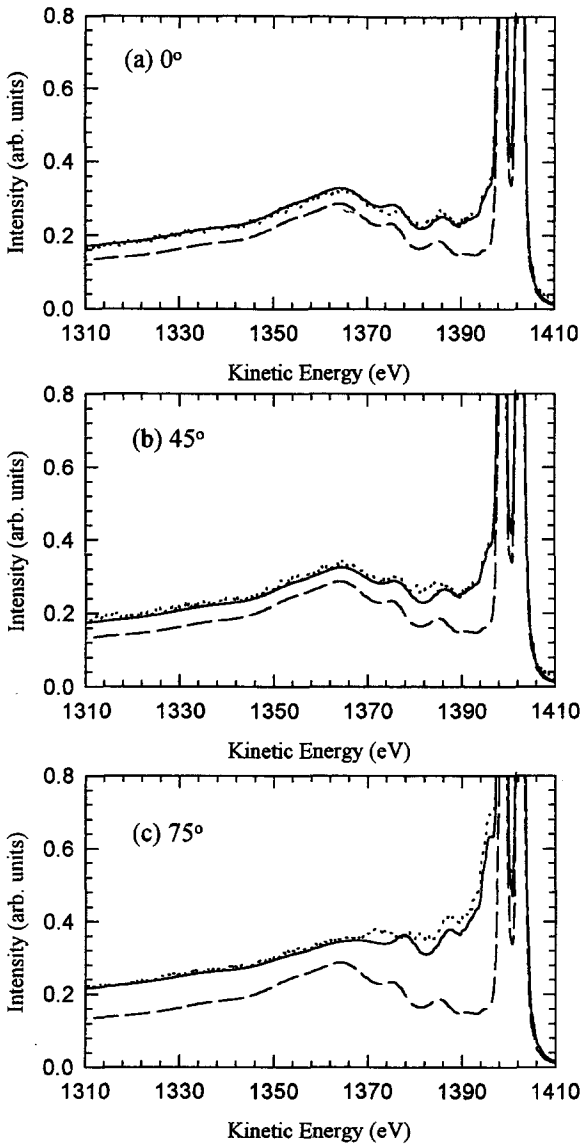

Fig. 6. A plot of Au 4f spectra calculated with (solid curve) and without (dashed curve) surface effects and those measured experimentally [24] (dotted curve) for different emission angles of (a) 0°, (b) 45°, and (c) 75°.

4. Conclusions

A dielectric response theory has been used to describe the interaction between the escape electron and the solid. A very general formula has been derived for the DIMFP of interest in XPS, AES and, in general, in any problem related to electrons interacting with surfaces. It was found that the DIMFP for electrons near a solid surface can be split up into a bulk and a surface term. The bulk term, which is spatially non-varying, gives rise to the DIMFP as in an infinite medium, whereas the position-dependent surface term is not confined to the interior of the solid but also takes place while the electron is outside where it must travel through the surface excitations. Inputting the present DIMFP into Monte Carlo simulations for Au 4f XPS spectra, the surface effects have been shown to be significant in XPS spectra. Moreover, the influence of surface excitations on the energy-loss structure within 30 eV is enhanced

for large take-off angles. Applying the spatial varying DIMFP in other forms of theoretical analysis in surface electron spectroscopy is currently underway.

References

[1] H.H. Madden and J.E. Houston, J. Appl. Phys. 47 (1976) 3071.
[2] C.J. Powell, in: Quantitative Surface Analysis of Materials, Ed. N.S. McIntyre, ASTM Special Technical Publication 643 (1978) p. 5.
[3] M.P. Seah, in: Scanning Electron Microscopy/1983, Vol. 2, Ed. O. Johari (SEM, AMF O'Hare, Illinois, 1983) p. 521.
[4] D.P. Woodruff and T.A. Delchar, Modern Techniques of Surface Science (Cambridge University Press, New York, 1986).
[5] N.H. Turner, Anal. Chem. 60 (1988) 377R.
[6] J.C. Riviere, Surface Analytical Techniques (Clarendon, Oxford, 1990).
[7] C.J. Powell, Surf. Sci. 44 (1974) 29.
[8] M.P. Seah and W.A. Dench, Surf. Interface Anal. 1 (1979) 2.
[9] S. Tanuma, C.J. Powell and D.R. Penn, Surf. Interface Anal. 11 (1988) 557.
[10] C.M. Kwei, Y.F. Chen, C.J. Tung and J.P. Wang, Surf. Sci. 293 (1993) 202.
[11] J.T. Grant, T.W. Hass and J.E. Houston, Phys. Lett. A 45 (1973) 309.
[12] P. Staib and J. Kirschner, Appl. Phys. 3 (1974) 421.
[13] D.A. Shirley, Phys. Rev. B 5 (1972) 4709.
[14] H.H. Madden and J.E. Houston, J. Appl. Phys. 47 (1976) 307.
[15] E.N. Sickafus, Surf. Sci. 100 (1980) 529.
[16] M.F. Koenig and J.T. Grant, J. Electron. Spectrosc. Relat. Phenom. 33 (1984) 9.
[17] S. Tougaard and P. Sigmund, Phys. Rev. B 25 (1982) 4452.
[18] A.L. Tofterup, Phys. Rev. B 32 (1985) 2808.
[19] V.M. Dwyer and J.A.D. Matthew, Surf. Sci. 193 (1988) 549.
[20] A.L. Tofterup, Surf. Sci. 227 (1990) 157.
[21] S. Tougaard, Phys. Rev. B 34 (1986) 6779.
[22] S. Tougaard and C. Jansson, Surf. Interface Anal. 20 (1993) 1013.
[23] S. Tougaard and I. Chorkendorff, Phys. Rev. B 25 (1987) 6570.
[24] S. Tougaard and J. Kraaer, Phys. Rev. B 43 (1991) 1651.
[25] F. Yubero and S. Tougaard, Phys. Rev. B 46 (1992) 2486.
[26] F. Yubero, J.M. Sanz, J.F. Trigo, E. Elizalde and S. Tougaard, Surf. Interface Anal. 22 (1994) 124.
[27] H. Yoshikawa, R. Shimizu and Z.J. Ding, Surf. Sci. 261 (1992) 403.
[28] H. Yoshikawa, T. Tsukamoto, R. Shimizu and V. Crist, Surf. Interface Anal. 18 (1992) 757.
[29] P.J. Feibelman, Surf. Sci. 36 (1973) 558.
[30] P.J. Feibelman, Phys. Rev. B 7 (1973) 2305.
[31] M. Kitagawa, Nucl. Instrum. Methods B 33 (1988) 409.
[32] Y.F. Chen, Surf. Sci. 345 (1996) 213.
[33] R.H. Ritchie and A.L. Marusak, Surf. Sci. 4 (1966) 234.
[34] F. Flores and F. Garcia-Moliner, J. Phys. C 12 (1979) 907.
[35] D. Chan and P. Richmond, J. Phys. C 9 (1976) 163.
[36] R.H. Ritchie, Phys. Rev. 106 (1957) 874.
[37] R.F. Egerton, Electron Energy-Loss Spectroscopy in the Electron Microscope (Plenum, New York, 1986).
[38] H. Raether, in: Excitations of Plasmons and Interband Transitions by Electrons, Springer Tracts in Modern Physics, Vol. 88, Ed. G. Höhler (Springer, New York, 1980).
[39] C.J. Powell, Phys. Rev. 175 (1968) 511.
[40] R.H. Ritchie and A. Howie, Philos. Mag. 36 (1977) 463.
[41] R.H. Ritchie, R.N. Hamm, J.E. Turner, H.A. Wright and W.E. Bolch, in: Physical and Chemical Mechanisms in Molecular Radiation Biology, Eds. W.A. Glass and M.N. Varma (Plenum, New York, 1991) p. 99.
[42] D.Y. Smith and E. Shiles, Phys. Rev. B 17 (1978) 4689.
[43] P.J. Feibelman, Prog. Surf. Sci. 12 (1982) 287.
[44] P.J. Feibelman, Phys. Rev. B 9 (1974) 5077.
[45] Y.F. Chen, C.M. Kwei and C.J. Tung, J. Phys. D Appl. Phys. 25 (1992) 262.
[46] Y.F. Chen, P. Su, C.M. Kwei and C.J. Tung, Phys. Rev. B 50 (1994) 17547.
[47] J.P. Wang, C.J. Tung, Y.F. Chen and C.M. Kwei, Nucl. Instrum. Methods B 108 (1996) 331.
[48] S. Doniach and M. Sunjic, J. Phys. C 3 (1970) 285.
[49] D.R. Penn, Phys. Rev. Lett. 38 (1977) 1429.